Zero Kinetic Energy (ZEKE) Photoelectron Spectroscopic Study of Thioanisole and Its van der Waals Complexes with Argon

Tomáš Vondrák,[†,‡] Shin-ichiro Sato,[†] Vladimír Špirko,[‡] and Katsumi Kimura*[,†]

School of Materials Science, Japan Advanced Institute of Science and Technology, Tatsunokuchi, Ishikawa 923-12, Japan, and J. Heyrovský Institute of Physical Chemistry, Academy of Sciences of Czech Republic, Dolejškova 3, 182 23 Prague 8, Czech Republic

Received: July 2, 1997; In Final Form: August 27, 1997[⊗]

Two-color zero kinetic energy (ZEKE) photoelectron spectra due to the cation D_0 states of thioanisole and its van der Waals complexes with argon (thioanisole−Ar and $-Ar_2$) in a supersonic jet are reported for the first time, together with mass-selected REMPI (resonantly enhanced multiphoton ionization) spectra associated with their S_1 states. For bare thioanisole, the adiabatic ionization energy (I_a) is 63 906 ± 3 cm^{-1} and the S_1 origin is located at 34 506 ± 1 cm^{-1}. Low-frequency vibrational progressions due to the excitation of the CH_3S torsion (94 cm^{-1}) are observed in the ZEKE photoelectron spectra. A series of hot bands showing a large anharmonicity is observed in a REMPI spectrum, indicating that the CH_3S torsional frequency is 68 cm^{-1} in the neutral ground state. An ab initio 6-311G** calculation gives a torsional barrier of 530 cm^{-1} along the S−C(sp^2) bond and a minimum energy for the CH_3 group rotated 90° from the aromatic plane. Intensive $\Delta v = 0$ ionization transitions are observed in the ZEKE photoelectron spectra via several S_1 vibronic levels. Concerning the thioanisole−Ar and $-Ar_2$ vdW complexes, the shifts in I_a amount to −117 and −231 cm^{-1}, respectively, with respect to thioanisole, while the shifts in the S_1 origin are −51 and −100 cm^{-1}, respectively. The vdW bending modes (b_x and b_y) in the S_1 states are resolved in the REMPI spectrum. The vdW b_x mode is observed up to $v = 5$ in the ZEKE photoelectron spectrum due to thioanisole−Ar.

Introduction

The conformation of aromatic ethers and thioethers is a topic of a fundamental interest.[1] A series of NMR studies of thioethers in solution indicate the presence of both a planar (**1**) and a perpendicular (**2**) conformer (see Chart 1).[2−7] For unsubstituted thioanisole, the planar conformation seems to be prevalent.

The relative stability of the two conformers is strongly affected by aromatic ring substituents. Variable-temperature IR and UV spectra of thioanisole derivatives were also interpreted in terms of the presence of two conformers.[8−10] However, there is a disagreement in the literature concerning the relative population of the two conformers and the height of the torsional barrier. A series of semiempirical and ab initio calculations also provided unequivocal results.[11,12] According to a recent interpretation of microwave spectra, the planar conformation (**1**) is present under free jet conditions.[13]

Electronic spectra of methoxybenzenes in a supersonic jet expansion have been studied by means of LIF (laser-induced fluorescence) spectroscopy,[14,15] by REMPI (resonantly enhanced multiphoton ionization) ion-current spectroscopy, from which direct information about structural conformation can be deduced,[16] and by two-color ZEKE (zero kinetic energy) photoelectron spectroscopy based on resonant ionization (or REMPI).[17,18] The effect of the side chain conformation on ZEKE photoelectron spectra is observable for the van der Waals (vdW) complexes of *cis*- and *trans*-*p*-dimethoxybenzene with argon.[19] The ZEKE photoelectron spectroscopy is also useful for studying the hindered rotation of the methyl group in the methylbenzene cations.[20−22]

Two-color ZEKE photoelectron spectroscopy is especially powerful to carry out high-resolution cation spectroscopy for jet-cooled molecular species.[23,24] Several applications of this technique in cation spectroscopy have earlier been demonstrated.[25] The selective population of a single intermediate state in the two-color REMPI scheme allows us to obtain selectively ZEKE photoelectron spectra of particular conformers present in the supersonic jet expansion. In the present study a compact cm^{-1}-resolution ZEKE photoelectron analyzer[26] was used, which has a high brightness due to a short flight distance of ZEKE electrons. This ZEKE analyzer has so far been extensively used to study a series of aromatic molecules exhibiting conformational isomerism as well as a series of argon vdW complexes of aromatic molecules showing low-frequency torsional modes and vdW vibrational modes.[27−34]

CHART 1

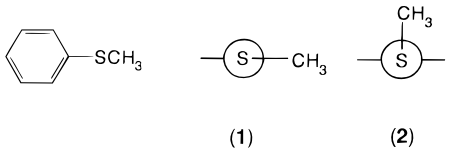

(**1**) (**2**)

To our best knowledge, literature data on electronic spectra of thioanisole are limited to the condensed phase. We report here one-color (1+1) REMPI ion-current spectra and two-color (1+1′) ZEKE photoelectron spectra of jet-cooled thioanisole for the first time, showing low-frequency vibrational structures in the neutral S_1 state and in the cation ground (D_0) state, respectively. The ZEKE photoelectron spectra obtained via several particular S_1 vibronic levels may provide a clue to distinguish the $S_1 \leftarrow S_0$ transitions of the different conformers. We also report experimental frequencies of the CH_3S torsional motion in the neutral and cation states, together with the theoretical ones which were obtained by solving a one-dimensional rigid-rotor wave equation with potential curves deduced from ab initio (6-311G**) calculations.

In van der Waals (vdW) complexes of a planar aromatic molecule with argon, there are two equivalent bonding sites on

[†] Japan Advanced Institute of Science and Technology.
[‡] J. Heyrovský Institute of Physical Chemistry.
* Corresponding author.
[⊗] Abstract published in *Advance ACS Abstracts,* October 15, 1997.

S1089-5639(97)02155-5 CCC: $14.00

the aromatic plane and an additive relation holds for the shifts of the S_1 and D_0 origins. On the other hand, for a nonplanar aromatic molecule with two nonequivalent bonding sites, it may result in a nonadditivity on the spectral shifts upon the complex formation with argon. We also report here two-color (1+1′) REMPI ion-current spectra and (1+1′) ZEKE photoelectron spectra of the thioanisole−Ar and $-Ar_2$ vdW complexes with the aim of obtaining further evidence on the conformation of thioanisole under free jet conditions.

Experimental and Computational Details

The experimental setup is essentially similar to that used in previous studies,[32−34] and only a brief description is given here. The supersonic free jet expansion is generated by a pulsed valve (General Valve) with an orifice diameter of 0.8 mm. The stagnation pressure was in the range 3−4 atm. Thioanisole (Extra Pure Grade) from Nacalai Tesque was used without further purification. The sample was degassed by repeated freeze/thaw cycles and seeded in argon or helium at room temperature.

The laser system consists of a Nd:YAG laser (Quanta-Ray GCR-190) pumping two dye lasers (Quanta Ray PDL-3). The outputs of the dye lasers were frequency doubled by KD*P crystals. A wavemeter (Burleigh Instruments, WA 5500) was used for a wavelength calibration of the dye lasers. The dyes Rhodamine 590 and 610 were used for the $S_1 \leftarrow S_0$ excitation, while LDS 698 and DCM were used for the ionization step ($D_0 \leftarrow S_1$). Counterpropagating laser beams were loosely focused by 200 mm focal length lenses into the ionization region. In measurements of MPI ion-current spectra, a one-color (1+1) ionization scheme was used for bare thioanisole, while a two-color (1+1′) scheme was used for the vdW complexes (thioanisole−Ar and $-Ar_2$). The ionizing laser was tuned approximately 100 cm^{-1} above the ionization threshold in order to avoid an extensive photofragmentation of the complexes. The MPI ion-current signals were mass selected by a 20 cm time-of-flight mass analyzer of a Wiley−McLaren type.[35]

A two-pulsed-field method was used for recording ZEKE photoelectron spectra.[36] The analyzer collecting ZEKE photoelectrons consists of two parallel electrodes. A repelling electric field V_1 applied approximately 50 ns after the laser shot prevents free electrons from reaching the electron multiplier. This field also ionizes high lying Rydberg states located a few cm^{-1} below the ionization threshold. Approximately 1 μs after the laser shot, the second pulsed field, $V_2 > V_1$, was applied in the opposite direction. This field ionizes the deeper lying Rydberg states and accelerates ZEKE electrons toward the detector. The "depth" of the field ionization is proportional to the square root of the intensity of the pulsed electric field, $\Delta E(cm^{-1}) \approx (4-6)V^{1/2}$. The typical field intensities were 0.7 and 1.2 V cm^{-1}, respectively. The measured ionization energies are biased by the Stark effect. The estimated red shift amounts to 4.6−6.8 cm^{-1} in the current experimental setup. The published values are not corrected for this shift.

Ab initio calculations were carried out with the Gaussian-94 program package[37] using the 6-311G** basis set. The UHF method was used for the cation ground state. A full geometry optimization was carried out. The effective torsional barrier was obtained by full geometry optimization for a given torsional angle. The purely torsional potential energy function was obtained for the molecule fixed at the optimum geometry as a function of the torsional angle only. The potential energy curve was calculated with an interval of 5° and was fitted by a cosine power series up to sixth order. The torsional (internal rotation) energies E_i and the corresponding wave functions Φ_i were obtained as eigenvalues and eigenfunctions, respectively, of the following one-dimensional Schrödinger equation,

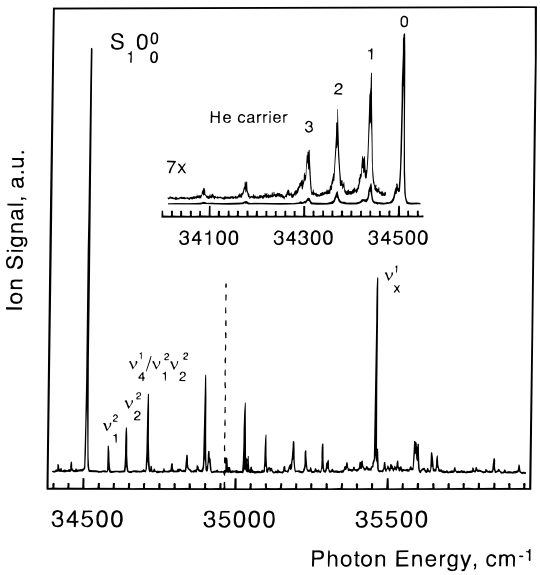

Figure 1. One-color (1+1) REMPI ion-current spectrum of thioanisole seeded in argon under free jet conditions. The two weak peaks on the red side of the S_1 origin are due to the thioanisole−Ar and $-Ar_2$ van der Waals complexes. The inset shows a detail of the spectrum obtained with the helium carrier gas. The change in the laser dye is shown by a broken line.

$$\left[-\frac{h^2}{8\pi^2}G_{tt}\frac{d^2}{d\Theta^2} + V(\Theta)\right]\Phi_i(\Theta) = E_i\Phi_i(\Theta) \qquad (1)$$

where h is the Planck constant and G_{tt} is the torsional part of the Wilson **G** matrix. The solution of eq 1 was obtained making use of the Numerov−Cooley integration procedure.[38]

Results and Discussion

Mass-Selected REMPI Spectra of Thioanisole. The one-color (1+1) REMPI ion-current spectrum of thioanisole (seeded in argon), observed in the range 34 400−35 950 cm^{-1}, is shown in Figure 1, in which the inset shows the spectrum obtained with a helium carrier gas in the region 34 000−34 540 cm^{-1}. The most intensive band at 34 506 cm^{-1} may be assigned to the S_1 origin of thioanisole, because no further structure was observed down to 33 000 cm^{-1}. The vibronic levels of the S_1 manifold in the region up to 1343 cm^{-1} are summarized in Table 1, together with their tentative vibrational assignments based on the ZEKE photoelectron spectra. (Two weak peaks appearing on the red side of the S_1 origin in Figure 1 obviously correspond to the thioanisole−Ar and $-Ar_2$ vdW complexes as follows from the mass spectra.) The Franck−Condon envelope corroborates identical conformations of the CH_3S moiety in the neutral ground and S_1 states.

The mass-resolved spectrum obtained with a helium carrier gas (the inset in Figure 1) indicates that the extended structure on the red side of the S_1 origin is due to hot bands (transitions from several vibrationally excited levels of the ground state) and not due to any vdW complexes of thioanisole with helium atoms. Helium is generally less effective in the cooling of vibrational and torsional motions. The observed vibrational progression exhibiting a strong anharmonicity is summarized in Table 2. The hot band structure is most likely due to the torsional motion of the CH_3S group with respect to the benzene ring.

TABLE 1: Vibronic Levels of the S_1 Manifold of Thioanisole

energy[a] (cm^{-1})	Δ from S_1 0^0 (cm^{-1})	assignment[b]
34 506	0	0^0
34 578	72	ν_1^2
34 637	131	ν_2^2
34 695	189	ν_3^1
34 708	202	$\nu_4^1/\nu_1^2\nu_2^2$
34 719	213	ν_5^1
34 730	224	$\nu_1^1\nu_3^1$
34 763	257	$\nu_1^2\nu_3^1$
34 788	282	$\nu_1^2\nu_5^1$
34 815	309	ν_6^1
34 838	332	$\nu_2^2\nu_4^1/\nu_1^2\nu_2^4$
34 874	368	ν_7^1
34 896	390	ν_8^1
34 910	404	$\nu_4^2/\nu_1^4\nu_2^4$
34 970	464	$\nu_1^2\nu_8^1$
34 979	473	$\nu_1^2\nu_4^2$
35 028	522	$\nu_2^2\nu_8^1$
35 041	535	$\nu_1^4\nu_8^1$
35 098	592	$\nu_4^1\nu_8^1/\nu_1^2\nu_2^2\nu_8^1$
35 190	684	
35 230	724	$\nu_2^2\nu_4^1\nu_8^1/\nu_1^2\nu_2^4\nu_8^1$
35 285	779	ν_8^2
35 459	953	ν_x^1
35 592	1085	$\nu_2^2\nu_x^1$
35 644	1138	
35 662	1156	$\nu_4^1\nu_x^1/\nu_x^1\nu_1^1\nu_2^1$
35 849	1343	$\nu_8^1\nu_x^1$

[a] Above 35 028 cm^{-1}($\nu_2^2\nu_8^1$), only intensive bands are included in this table. [b] Assignments of bands up to 35 028 cm^{-1} are supported by ZEKE photoelectron spectra obtained via the particular levels.

TABLE 2: Experimental and Calculated Energy Levels (in cm^{-1}) for the Torsional Motion along the S−C(sp^2) Bond

		calculated[b]			
υ_t	observed[a]	σ_T[c]	σ_C[c]	relaxed[d]	frozen[e]
0	0	s, a[f]	s, a[f]	0	0
1	68	s, a	s, a	62.1	59.9
2	138	s, a	s, a	122.8	125.3
3	198	s, a	s, a	182.7	190.5
4		s, a	s, a	240.1	255.1
5		s, a	s, a	294.8	320.1
6		s, a	s, a	345.8	385.1
7		s, a	s, a	392.5	450.8
8		s	s	433.652	516.524
8		s	a	433.655	516.524
8		a	a	433.658	516.524

[a] From the spectrum shown in the inset in Figure 1. [b] The potential energy functions shown in Figure 2 are used. [c] The same notation used as in ref 39. [d] Calculated by using the effective torsional potential energy function. [e] Calculated by using the purely torsional potential energy function. [f] Internal rotation splitting smaller than 10^{-3} cm^{-1}.

Two kinds of potential energy curves (solid and dashed lines) are shown in Figure 2, which were obtained from the present ab initio calculations using the 6-311G** basis set, indicating a single potential energy minimum at the perpendicular conformation (**2**) and a relaxed torsional barrier of 530 cm^{-1} (solid line). The purely torsional barrier given by a dashed line in Figure 2 amounts to 1180 cm^{-1}. The relaxation is mainly on account of a shortening of the S−C(sp^2) bond length and an increasing of the C−S−C(sp^2) angle. Torsional energy levels calculated with both the "relaxed" and "purely rotational" potential energy curves are compared with the observed ones in Table 2.

Mass-Selected REMPI Spectra of Thioanisole−Ar and −Ar_2. Two-color (1+1′) mass-resolved REMPI ion-current spectra obtained for the thioanisole−Ar and −Ar_2 vdW complexes are presented in Figure 3, showing intense peaks

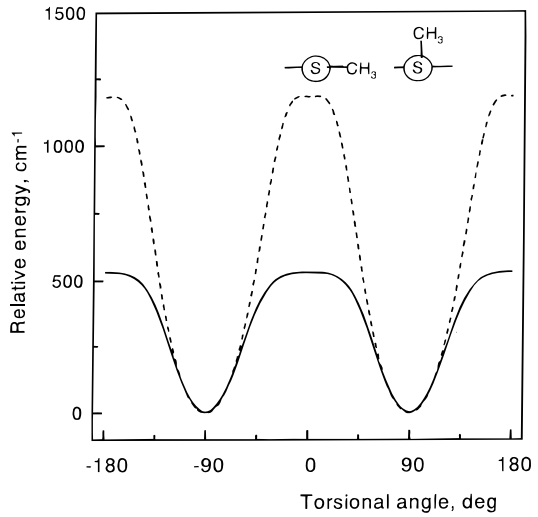

Figure 2. Calculated torsional barriers for rotation of the CH_3S group about the S−C(sp^2) bond. The solid line represents the relaxed barrier where the geometry is optimized at each value of the torsional angle. The dashed line indicates the purely rotational barrier where only the torsional angle is varied.

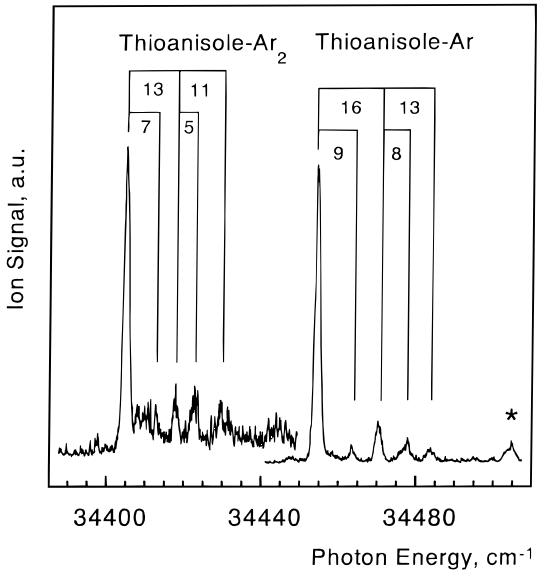

Figure 3. Two-color mass-selected (1+1′) REMPI ion-current spectra of the thioanisole−Ar and −Ar_2 van der Waals complexes. The S_1 origins of thioanisole−Ar and −Ar_2 are shifted by −51 and −100 cm^{-1}, respectively, with respect to bare thioanisole. The band marked by an asterisk is due to bare thioanisole.

attributable to their S_1 origins at 34 455 and 34 406 cm^{-1}, respectively, with several low-frequency vibrational bands. The S_1 origins of thioanisole−Ar and −Ar_2 are shifted by −51 and −100 cm^{-1}, respectively, from that of bare thioanisole. The latter shift is just twice as much the former within experimental error. This additive character in the red shift strongly suggests that the thioanisole moiety is effectively planar, and thus both sides are equivalent.

The frequencies of vdW bending modes in several vdW complexes of aromatic molecules with argon in the S_1 state are reported to be 10−16 cm^{-1}.[40−45] The vibrational structures observed in Figure 3 may be interpreted in terms of vdW vibrational modes. There should be a total of three and six vdW vibrational modes in thioanisole−Ar and −Ar_2, respectively. In the spectrum of thioanisole−Ar, a weak peak appearing at 9 cm^{-1} from the origin band may tentatively be assigned to one quantum of the vdW bending mode (b_x^1) along

TABLE 3: Van der Waals Vibrational Transitions Observed in the Neutral S_1 State and Cation D_0 State of Thioanisole−Ar and $-Ar_2$

	S_1		D_0	
	vibr freq (cm^{-1})	assignt[a]	vibr freq (cm^{-1})	assignt
thioanisole−Ar	0	0^0	0	0^0
	9	b_x^1	11	b_x^1
	16	b_y^1	18	b_x^2
	24	$b_y^1 b_x^1$	29	b_x^3
	29	b_y^2	39	b_x^4
			50	b_x^5
thioanisole−Ar_2	0	0^0		
	7	b_{xs}^1		
	13	b_{ys}^1		
	18	$b_{ys}^1 b_{xs}^1$		
	24	b_{ys}^2		

[a] vdW bending modes (the aromatic ring is in the $x-y$ plane; the C−S bond is on the x axis).

the S−C(sp^2) bond (the x axis). The next peak appearing at 16 cm^{-1} may be assigned to the one-quantum transition of another vdW bending mode (b_y) rather than to the b_x^2 level, because of its relative intensity. (The benzene ring is in the $x-y$ plane and the C−S bond lies on the x axis.) The two additional bands appearing at 24 (=16 + 8) cm^{-1} and 29 (=16 + 13) cm^{-1} may originated from the $b_x^1 b_y^1$ and b_y^2 levels, respectively.

Analogously, the spectrum of thioanisole−Ar_2 (Figure 3) shows two weak peaks at 7 and 13 cm^{-1}, which may be due to the two "symmetric" bending modes, b_{xs} and b_{ys}, respectively. The coordination of the second Ar atom results in the decrease of the vdW frequencies. All the low-frequency bands assignable to the vdW vibrational progressions (Figure 3) are summarized in Table 3.

ZEKE Photoelectron Spectra of Thioanisole. Figure 4 shows four ZEKE photoelectron spectra of bare thioanisole, which were obtained via the S_1 origin and three low-frequency vibronic levels (S_1 ν_1^2, ν_2^2, and $\nu_4^1/\nu_1^2\nu_2^2$). Vibrational bands observed in the ZEKE spectra (Figure 4) are summarized in Table 4, together with the possible vibrational assignments of the thioanisole cation.

The strong lowest energy band appearing at 63 906 cm^{-1} in spectrum a in Figure 4 may safely be assigned to the vibrationless ground cation state (D_0). It gives the adiabatic ionization energy (I_a = 63 906 ± 5 cm^{-1}; 7.9234 eV ± 0.0004 eV). Two kinds of vibrational progressions are observed in Figure 4a; one is a vibrational progression with a frequency of 94 cm^{-1} up to $v = 4$, and the other is a progression with a frequency of 152 cm^{-1} up to $v = 2$. Another weak band appearing at 245 cm^{-1} in Figure 4a fits the $\nu_1^1\nu_2^1$ combination. The Franck−Condon envelope of the $D_0 \leftarrow S_1(0_0^0)$ transition indicates a close geometry of these two states (D_0 and S_1).

The spectrum in Figure 4b, obtained via the first excited vibrational level (S_1 ν_1^2), shows three strong transitions to the cation D_0 0^0, ν_1^2, and $\nu_1^1\nu_2^1$ levels. In the planar conformation (**1**), the C_s symmetry dictates the even selection rule $\Delta v = 0$, 2, ... for the out-of-plane modes. Given the $\Delta v = 0$ propensity observed for the transitions from the S_1 origin, the higher intensities of the 0_0^0 and ν_1^2 bands compared to the ν_1^1 band in Figure 4b may indicate that the ionization transitions take place from an even level of a non-totally symmetric mode. Thus the lower state of these ionization transitions may tentatively be assigned to the S_1 ν_1^2 level. The strong 0_0^0 peak may be due to a dramatic narrowing of the torsional potential energy function in the cation state. A similar situation also occurs in the ionization taking place via the second excited level of S_1 (Figure 4c). Analogously the intermediate state is assigned

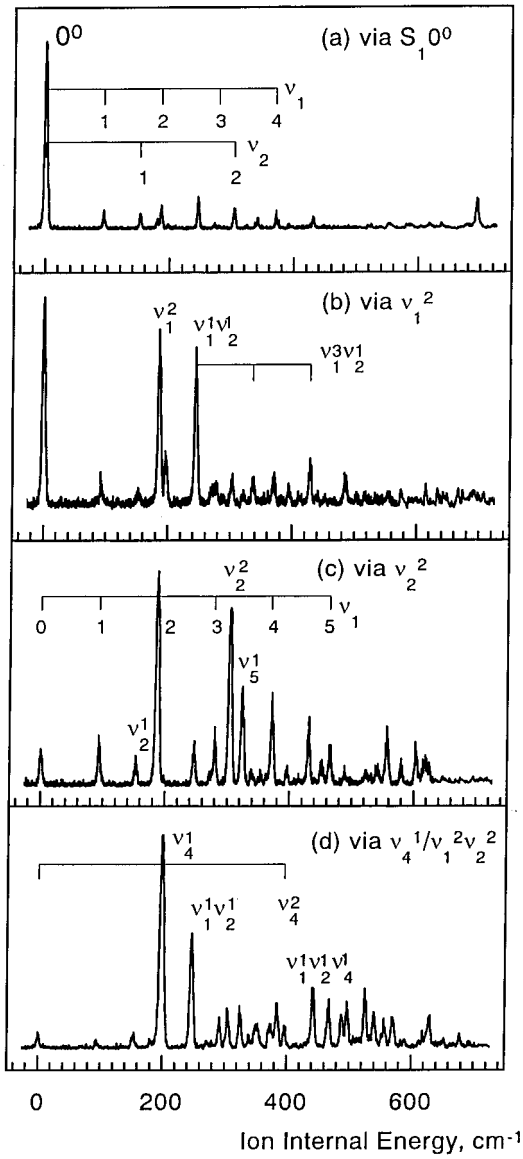

Figure 4. ZEKE photoelectron spectra of thioanisole, obtained via (a) S_1 0^0, (b) S_1 ν_1^2, (c) $S_1\nu_2^2$, and (d) S_1 $\nu_4^1/\nu_1^2\nu_2^2$, showing the cation vibrational spectra. For band assignments see Table 3.

to the S_1 ν_2^2 level. The cation band assigned to ν_2^1 is considerably weaker than the ν_2^2 band. The vertical transition is to the D_0 ν_1^2 level. The harmonic analysis indicates that the two lowest energy vibrational modes (ν_1 and ν_2) have a large CH_3S−C(sp^2) torsional contribution and differ from each other mainly in the phase of the CH_3 group torsional motion around the CH_3−S bond. A large change in the torsional potential manifests itself in the ν_1^2 population upon the ionization of the S_1 ν_2^2 state.

The fourth excited vibronic level of S_1 fits the $\nu_1^2\nu_2^2$ combination (see Table 1). As seen from spectrum d obtained via this level (Figure 4), the vertical transition gives a frequency of 198 cm^{-1}. The $\nu_1^1\nu_2^1$ combination band appearing at 246 cm^{-1} is slightly weaker in intensity. Therefore it may be justified that the S_1 band at 202 cm^{-1} is tentatively assigned to an overlap of a fundamental ν_4 level with a $\nu_1\nu_2$ combination level.

Further measurements of ZEKE photoelectron spectra of thioanisole were carried out by selecting weaker and higher energy REMPI ion-current peaks (see Figure 1) corresponding to the following higher S_1 levels: namely, (a) ν_3^1, (b) ν_5^1, (c) $\nu_1^1\nu_3^1$, (d) $\nu_1^2\nu_3^1$, (e) $\nu_1^2\nu_5^1$, (f) $\nu_1^2\nu_2^4/\nu_2^2\nu_4^1$, (g) ν_7^1, (h) ν_8^1,

TABLE 4: Vibrational Frequencies of Thioanisole in Cation D_0 State, Obtained from ZEKE Photoelectron Spectra, and Their Vibrational Assignments

ion internal energy, cm^{-1}	assignt	ion internal energy, cm^{-1}	assignt
	(**a**) via $S_1\ 0_0^0$		
0	0^0	279	ν_1^3
94	ν_1^1	304	ν_2^2
152	ν_2^1	324	ν_5^1
179	ν_3^1	338	$\nu_1^2\nu_2^1$
186	ν_1^2	371	ν_1^4/ν_6^1
197	ν_4^1	396	$\nu_4^2/\nu_1^1\nu_2^2$
245	$\nu_1^1\nu_2^1$	431	$\nu_1^3\nu_2^1/\nu_7^1$
271	$\nu_1^1\nu_3^1$		
	(**b**) via $S_1\ \nu_1^2$		
0	0^0	323	ν_5^1
93	ν_1^1	337	$\nu_1^2\nu_2^1$
152	ν_2^1	370	ν_1^4/ν_6^1
179	ν_3^1	382	$\nu_1^2\nu_4^1$
186	ν_1^2	394	$\nu_4^2/\nu_1^1\nu_2^2$
196	ν_4^1	429	$\nu_1^3\nu_2^1/\nu_7^1$
245	$\nu_1^1\nu_2^1$	487	$\nu_1^2\nu_2^2/\nu_1^1\nu_4^2$
271	$\nu_1^1\nu_3^1$	503	$\nu_3^1\nu_5^1/\nu_2^2\nu_4^1$
278	ν_1^3	517	$\nu_1^2\nu_2^1\nu_3^1$
288	$\nu_1^1\nu_4^1$		
303	ν_2^2		
	(**c**) via $S_1\ \nu_2^2$		
0	0^0	415	$\nu_1^1\nu_5^1$
94	ν_1^1	431	$\nu_1^3\nu_2^1/\nu_7^1$
153	ν_2^1	452	$\nu_1^1\nu_3^2$
187	ν_1^2	465	$\nu_1^5/\nu_1^1\nu_6^1$
247	$\nu_1^1\nu_2^1$	489	$\nu_1^2\nu_2^2/\nu_1^1\nu_4^2$
271	$\nu_1^1\nu_3^1$	524	$\nu_1^4\nu_2^1/\nu_2^1\nu_6^1/\nu_1^1\nu_7^1$
280	ν_1^3	541	$\nu_2^2\nu_4^1$
304	ν_2^2	557	$\nu_1^6/\nu_1^2\nu_6^1$
324	ν_5^1	580	$\nu_1^3\nu_2^2/\nu_2^1\nu_7^1$
338	$\nu_1^2\nu_2^1$	603	$\nu_1^3\nu_5^1$
353	$\nu_2^1\nu_4^1$		
372	ν_1^4/ν_6^1		
	(**d**) via $S_1\ \nu_4^1/\nu_1^2\nu_2^2$		
0	0^0	372	ν_1^4/ν_6^1
93	ν_1^1	383	$\nu_1^2\nu_4^1$
152	ν_2^1	395	$\nu_4^2/\nu_1^1\nu_2^2$
180	ν_3^1	441	$\nu_1^1\nu_2^1\nu_4^1$
198	ν_4^1	466	$\nu_1^5/\nu_1^1\nu_6^1$
246	$\nu_1^1\nu_2^1$	488	$\nu_1^2\nu_2^2/\nu_1^1\nu_4^2$
270	$\nu_1^1\nu_3^1$	495	ν_8^1
278	ν_1^3	525	$\nu_1^4\nu_2^1/\nu_2^1\nu_6^1/\nu_1^1\nu_7^1$
291	$\nu_1^1\nu_4^1$	537	$\nu_1^2\nu_2^1\nu_4^1$
304	ν_2^2	555	$\nu_1^6/\nu_1^2\nu_6^1$
324	ν_5^1	569	$\nu_1^1\nu_2^1\nu_5^1/\nu_1^4\nu_4^1/\nu_4^1\nu_6^1$
338	$\nu_1^2\nu_2^1$	628	$\nu_1^3\nu_2^1\nu_4^1/\nu_4^1\nu_7^1$
352	$\nu_2^1\nu_4^1$	651	$\nu_5^2/\nu_1^3\nu_6^1$

(i) $\nu_4^2/\nu_1^4\nu_2^4$, and (j) $\nu_1^2\nu_8^1$. The cation vibrational levels thus obtained from dominant ZEKE photoelectron bands are summarized in Table 5, together with their tentative cation vibrational assignments.

It is interesting to mention that the assignment of the weak 189 cm^{-1} REMPI band to the ν_3 fundamental mode of S_1 in Table 1 is supported by the appearance of the vertical ZEKE band due to the $\nu_1^1\nu_3^1$ cation level at 271 cm^{-1} (Table 5a). The photoelectron spectra obtained via $S_1\ \nu_5^1$, $\nu_1^2\nu_5^1$, and ν_7^1 levels show intensive peaks which fit formally to ν_1^4, ν_1^5, and ν_1^6 and their combinations with other modes (see Table 5b,e,g). Because of the symmetry the ν_1^5 transition should be weaker than the even ones, as was observed for the ν_1^2 level ionization. Therefore the strongest vertical band at 464 cm^{-1} (obtained via $S_1\ \nu_1^2\nu_5^1$) in Table 5e is assigned to the cation $\nu_1^1\nu_6^1$ vibrational level rather than the ν_1^5 level. In the same way the strongest vertical band at 430 cm^{-1} (obtained via $S_1\ \nu_8^1$) in Table 5h is assigned to the cation ν_7^1 level rather than the $\nu_1^3\nu_2^1$ level. The experimental fundamental frequencies of thioanisole in the S_1 and D_0 states thus obtained are summarized in Table 6 together with those calculated from a harmonic analysis for the cation D_0 state. As seen from Table 6, there is a reasonable agreement between the experiment and the calculation for the four lowest vibrational frequencies in the cation D_0 state.

There are nearly 3-fold increases in the ν_1 and ν_2 frequencies upon ionization, as seen from Table 6. This result indicates that the torsional barrier in the cation D_0 state is much steeper. The positive hole in the benzene π system brings about a stronger conjugation with the sulfur p_z orbital. The conjugation is the maximum at the planar (**1**) conformation. Given the Franck−Condon envelope for the $S_1 \leftarrow S_0$ excitation step and for the $D_0\ 0_0^0 \leftarrow S_1\ 0_0^0$ ionization, the planar conformation seems to be dominant under the free jet conditions.

The UHF 6-311G** calculation of the thioanisole cation gives a global minimum at the planar conformation (**1**). The electronic spectrum does not exhibit any transitions due to vibronic levels of another conformer, presumably the perpendicular one (**2**). The ZEKE photoelectron spectra corroborate the assignment of the observed S_1 levels to a single conformer.

ZEKE Photoelectron Spectra of Thioanisole−Ar and −Ar_2. A ZEKE photoelectron spectrum of the thioanisole−Ar vdW complex obtained via the S_1 band origin is shown in the region 63 760−63 880 cm^{-1} in Figure 5, indicating a vibrational progression with several well-resolved peaks. The vibrational interval amounts to 7−11 cm^{-1} and exhibits a visible anharmonicity (see Table 3). For the thioanisole−Ar_2 vdW complex, only a photoionization efficiency curve was recorded, since a broad unresolved feature was observed in a ZEKE photoelectron spectrum probably due to an overlap with a signal from a dimer species.

The adiabatic ionization energies of the vdW complexes were determined to be I_a (thioanisole−Ar) = 63 789 cm^{-1} and I_a (thioanisole−Ar_2) = 63 675 cm^{-1} from the first peak of the progression shown in Figure 5 and the mass-selected photoionization threshold obtained by the (1+1′) excitation, respectively. The I_a values of thioanisole and its −Ar and −Ar_2 vdW complexes are summarized in Table 7. The shifts in I_a from bare thioanisole are $\Delta I_a = -117$ and -231 cm^{-1} for thioanisole−Ar and −Ar_2, respectively. Thus, the I_a shift of thioanisole−Ar is almost twice that of thioanisole−Ar_2. A similar situation occurs in the aniline−Ar and −Ar_2 vdW complexes,[30] in which the additivity rule holds almost strictly for ΔI_a; namely, ΔI_a(aniline−Ar) = −111 cm^{-1} and ΔI_a(aniline−Ar) = −219 cm^{-1}. The additivity of the I_a shift suggests that there are two equivalent bonding sites on both sides of the aromatic moiety. This fact corroborates the planar conformation (**1**) also in the cation D_0 state.

The I_a shift of −117 cm^{-1} found for thioanisole−Ar is close to that of −111 cm^{-1} for aniline−Ar. For unsubstituted benzene, ΔI_a(benzene−Ar) is −172 cm^{-1}.[24] The data obtained recently in this laboratory for substituted benzenes (C_6H_5−CN,[33] C_6H_5−F,[46] C_6H_5−OCH_3[18]) show that the electron-donating substituents tend to destabilize the cation state relative to unsubstituted benzene. The I_a shift in a vdW complex may be written as

$$\Delta I_a = \Delta\nu_{ind} + \Delta\nu_{dis} \qquad (2)$$

where $\Delta\nu_{ind}$ represents the shift brought about by the induced dipole−charge interaction and $\Delta\nu_{disp}$ is the contribution of the dispersion interaction.[47] In cations, $\Delta\nu_{ind}$ is considered of a comparable magnitude as the dispersion component, whereas in neutral states $\Delta\nu_{ind}$ contributes about 5% to the spectral shift.[48] Obviously the electron flux from the electron-donating sub-

TABLE 5: Dominant ZEKE Photoelectron Bands of Thioanisole, Obtained via Weaker and Higher Energy Intermediate Levels

ion internal energy, cm^{-1}	intensity[a]	assignt	ion internal energy, cm^{-1}	intensity[a]	assignt
		(a) via $S_1\ \nu_3^1$			
197	55	ν_4^1	340	20	$\nu_1^2\nu_2^1$
245	59	$\nu_1^1\nu_2^1$	352	35	$\nu_2^1\nu_4^1$
271	100	$\nu_1^1\nu_3^1$	452	20	$\nu_1^1\nu_3^2$
322	39	ν_5^1			
		(b) via $S_1\ \nu_5^1$			
93	23	ν_1^1	370	20	ν_1^4/ν_6^1
186	40	ν_1^2	465	100	$\nu_1^5/\nu_1^1\nu_6^1$
197	70	ν_4^1	525	67	$\nu_1^4\nu_2^1/\nu_2^1\nu_6^1/\nu_1^1\nu_7^1$
245	22	$\nu_1^1\nu_2^1$	555	20	$\nu_1^6/\nu_1^2\nu_6^1$
271	26	$\nu_1^1\nu_3^1$	614	21	$\nu_1^5\nu_2^1/\nu_1^1\nu_2^1\nu_6^1$
		(c) via $S_1\ \nu_1^1\nu_3^1$			
93	38	ν_1^1	371	52	ν_1^4/ν_6^1
186	36	ν_1^2	465	69	$\nu_1^5/\nu_1^1\nu_6^1$
198	30	ν_4^1	525	28	$\nu_1^4\nu_2^1/\nu_2^1\nu_6^1/\nu_1^1\nu_7^1$
245	100	$\nu_1^1\nu_2^1$	554	38	$\nu_1^6/\nu_1^2\nu_6^1$
303	28	ν_2^2	615	27	$\nu_1^5\nu_2^1/\nu_1^1\nu_2^1\nu_6^1$
325	20	ν_5^1			
		(d) via $S_1\ \nu_1^2\nu_3^1$			
181	22	ν_3^1	340	37	$\nu_1^2\nu_2^1$
186	21	ν_1^2	353	54	$\nu_2^1\nu_4^1$
245	23	$\nu_1^1\nu_2^1$	453	25	$\nu_1^1\nu_3^2$
270	100	$\nu_1^1\nu_3^1$	466	60	$\nu_1^5/\nu_1^1\nu_6^1$
304	70	ν_2^2	526	55	$\nu_1^4\nu_2^1/\nu_2^1\nu_6^1/\nu_1^1\nu_7^1$
325	50	ν_5^1			
		(e) via $S_1\ \nu_1^2\nu_5^1$			
197	34	ν_4^1	464	100	$\nu_1^5/\nu_1^1\nu_6^1$
323	20	ν_5^1	486	29	$\nu_1^2\nu_2^2/\nu_1^1\nu_4^2$
352	23	$\nu_2^1\nu_4^1$	494	22	ν_8^1
371	22	ν_1^4/ν_6^1	524	79	$\nu_1^4\nu_2^1/\nu_2^1\nu_6^1/\nu_1^1\nu_7^1$
428	23	$\nu_1^3\nu_2^1/\nu_7^1$	554	20	$\nu_1^6/\nu_1^2\nu_6^1$
		(f) via $S_1\ \nu_1^2\nu_2^4/\nu_2^2\nu_4^1$			
322	44	ν_5^1	524	20	$\nu_1^4\nu_2^1/\nu_2^1\nu_6^1/\nu_1^1\nu_7^1$
340	100	$\nu_1^2\nu_2^1$	549	24	$\nu_1^1\nu_2^3$
351	21	$\nu_2^1\nu_4^1$			
		(g) via $S_1\ \nu_7^1$			
304	29	ν_2^2	553	55	$\nu_1^6/\nu_1^2\nu_6^1$
352	37	$\nu_2^1\nu_4^1$	693	28	$\nu_5^1\nu_6^1$
371	51	ν_1^4/ν_6^1	716	46	
535	47	$\nu_1^2\nu_2^1\nu_4$	743	100	ν_6^2
		(h) via $S_1\ \nu_8^1$			
0	35	0^0	577	34	$\nu_1^3\nu_2^2/\nu_2^1\nu_7^1$
352	20	$\nu_1^4\nu_2^1$	669	26	$\nu_1^4\nu_2^2/\nu_1^1\nu_2^1\nu_7^1$
430	100	$\nu_1^3\nu_2^1/\nu_7^1$	733	21	$\nu_1^3\nu_2^3/\nu_2^1\nu_7^1$
517	47	$\nu_1^3\nu_2^1\nu_3^1/\nu_1^1\nu_7^1$	859	21	ν_7^2
		(i) via $S_1\ \nu_4^2/\nu_1^4\nu_2^4$			
341	63	$\nu_1^2\nu_2^1$	505	44	$\nu_3^1\nu_5^1/\nu_2^2\nu_4^1$
383	57	$\nu_1^2\nu_4^1$	519	75	$\nu_1^2\nu_2^1\nu_3^1$
395	100	$\nu_4^2/\nu_1^1\nu_2^2$	537	21	$\nu_1^2\nu_2^1\nu_4^1$
431	86	$\nu_1^3\nu_2^1/\nu_7^1$	550	23	$\nu_2^1\nu_4^2$
454	20	$\nu_1^1\nu_3^2$	556	27	$\nu_1^6/\nu_1^2\nu_6^1$
466	21	$\nu_1^5/\nu_1^1\nu_6^1$	578	48	$\nu_1^3\nu_2^2/\nu_2^1\nu_7^1$
489	27	$\nu_1^2\nu_2^2/\nu_1^1\nu_4^2$	762	21	$\nu_1^2\nu_4^2$
494	24	ν_8^1			
		(j) via $S_1\ \nu_1^2\nu_8^1$			
432	82	$\nu_1^3\nu_2^1/\nu_7^1$	678	60	$\nu_1^1\nu_2^1\nu_7^1$
523	32	$\nu_1^4\nu_2^1/\nu_2^1\nu_6^1/\nu_1^1\nu_7^1$	705	46	$\nu_1^3\nu_7^1$
580	65	$\nu_1^3\nu_2^2/\nu_2^1\nu_7^1$	769	39	$\nu_1^2\nu_2^1\nu_7^1$
619	100	$\nu_1^2\nu_7^1/\nu_1^5\nu_2^1/\nu_1^1\nu_2^1\nu_6^1$	860	37	ν_7^2

[a] Only the bands of relative intensities greater than 20% are included in this table.

stituent tends to neutralize the positive hole on the aromatic ring and thus decreases the $\Delta\nu_{ind}$ contribution. On the other hand, the electron-withdrawing CN group increases ΔI_a by one-half relative to the unsubstituted benzene. The effect of the CH_3S group is very close to that of the NH_2 group ($\Delta I_a = -111$ cm^{-1}). A similar charge distribution may be anticipated in the cation state.

The low-frequency vibrational progression in Figure 5 may be interpreted in terms of one of the cation vdW vibrations. In the thioanisole−Ar cation, there are three vdW vibrations: namely, two bending and one stretching. Similar progressions of the vdW bending vibrations with frequencies of 12 and 16 cm^{-1} have previously been observed for the aniline−Ar cation[30] and the benzonitrile−Ar cation,[33] respectively. These frequen-

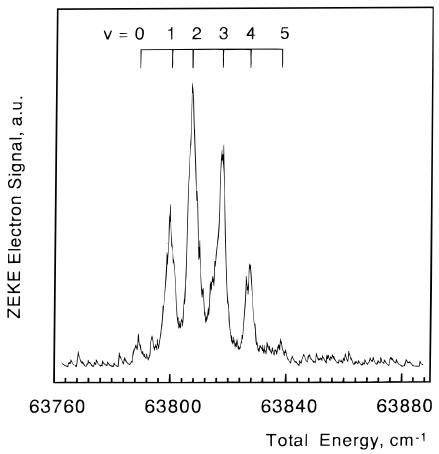

Figure 5. ZEKE photoelectron spectrum of the thioanisole−Ar vdW complex, obtained via the S_1 band origin, showing a well-resolved vibrational progression due to the b_x vdW bending mode of the cation.

TABLE 6: Vibrational Frequencies of Thioanisole in the Neutral S_1 State and in the Cation Ground State (D_0)

S_1 state		D_0 state		
exptl (cm^{-1})	assignt	exptl (cm^{-1})	calcd (cm^{-1})	assignt
36	ν_1	94	105	ν_1
66	ν_2	152	165	ν_2
189	ν_3	179	199	ν_3
202	ν_4	197	210	ν_4
213	ν_5	324	368	ν_5
309	ν_6	372	397	ν_6
368	ν_7	431	462	ν_7
390	ν_8	495	464	ν_8
953	ν_x			

TABLE 7: S_1 Origins and Adiabatic Ionization Energies of Thioanisole and Thioanisole−Ar and $-Ar_2$ VdW Complexes

	S_1 0_0^0 (cm^{-1})	$\Delta\nu$ (cm^{-1})	I_a (cm^{-1})	ΔI_a (cm^{-1})
thioanisole	34 506		63 906	
thioanisole−Ar	34 455	−51	63 789	−117
thioanisole−Ar_2	34 406	−100	63 675[a]	−231

[a] Value obtained from a photoionization efficiency curve.

cies are assigned to the vdW bending mode along the *x* axis (the direction of the S−C(sp^2) bond). An identical assignment may be adopted for the thioanisole−Ar cation.

Conclusions

From both the mass-selected REMPI and ZEKE photoelectron experiments, accurate values of the S_1 origins and the adiabatic ionization energies (I_a) have been determined for thioanisole as well as for the thioanisole−Ar and $-Ar_2$ vdW complexes, and several low-frequency fundamental vibrations (including the CH_3S torsional motions) up to 500 cm^{-1} have been identified for bare thioanisole in the neutral S_1 and cation D_0 states. The vibrational assignment of some S_1 bands of thioanisole to its fundamental vibrational modes is supported by the ZEKE photoelectron spectra obtained via the particular S_1 levels. From the present study it may be concluded that only a single conformer is present under free jet conditions. The CH_3S group torsional angles in thioanisole in the S_0, S_1, and D_0 states are identical with one another. The planarity of thioanisole is supported by the additive relations in the observed energy shifts both in the S_1 origins and in the adiabatic ionization energies of the thioanisole−Ar and $-Ar_2$ vdW complexes.

The HF ab initio 6-311G** calculation predicts the planar conformation (**1**) in the thioanisole cation D_0 state. In the neutral S_0 state, a minimum is predicted for the perpendicular conformation of the CH_3S group with a 2-fold torsional barrier of 530 cm^{-1}. Although there is a reasonable agreement between the calculated torsional levels and the experimental ones deduced from the hot band structure, the balance between the π conjugation and the steric effect seems to be not properly assessed at this level.

In the present study the potentiality of two-color REMPI and ZEKE photoelectron spectroscopy has been demonstrated in studying the conformational structure of the flexible molecule as well as in observing the series of low-frequency vdW vibrations. It should be mentioned that the observation of the vdW complexes of aromatic molecules with rare gas atoms is also useful for the determination of the conformation of the aromatic moiety.

Acknowledgment. T.V. wishes to thank the Japan Society for the Promotion of Science for the financial support for his stay at Japan Advanced Institute of Science and Technology as a Visiting Researcher during the period of this work (Foreign Researchers Invitation Program), and also thanks the Grant Agency of the Czech Republic for the financial support under Grant No. 203/95/1056. V.S. gratefully acknowledges the financial support from the Grant Agency of the Czech Republic, Grant No. A4040501. This work was partly supported by a Grant-in-Aid from the Ministry of Education, Science, Sports and Culture of Japan (K.K.; Scientific Research C: No. 06640468).

References and Notes

(1) Allen, G.; Fewster, S. *Internal Rotations in Molecules*; Orwille-Thomas, W. J., Ed; Wiley: New York, 1974; Chapter 8.
(2) Bzhezovsky, V. M.; Penkovsky V. V.; Rozhenko, A. B.; Iksanova, S. V.; Kondratenko, N. V.; Yagupolsky, L. M. *J. Fluorine Chem.* **1994**, *69*, 41.
(3) Lumbroso, H.; Liegéois, C.; Testaferri, L.; Tiecco, M. *J. Mol. Struct.* **1986**, *144*, 121.
(4) Schaeffer, T.; Penner, G. H. *Can. J. Chem.* **1988**, *66*, 1229.
(5) Schaeffer, T.; Baleja J. D. *Can. J. Chem.* **1986**, *64*, 1376.
(6) Schaeffer, T.; Penner, G. H. *Can. J. Chem.* **1988**, *66*, 1641.
(7) Schaeffer, T.; Sebastian R.; Salman, S. R.; Baleja, J. D.; Penner, G. H., McKinnon, D. M. *Can. J. Chem.* **1991**, *69*, 620.
(8) Shivernovskaya, O. A.; Ratovskii, G. V. *Zh. Obsch. Khim.* **1993**, *63*, 2342.
(9) Shivernovskaya, O. A.; Ratovskii, G. V.; Kondratenko, N. V.; Boiko, V. N. *Ukr. Khim. Zh.* **1992**, *58*, 687.
(10) Panov, A. M.; Ratovskii, G. V.; Chuvasnev, D. D.; Shivernovskaya, O. A. *Zh. Obsch. Khim.* **1983**, *53*, 517.
(11) Dolenko, G. N.; Litvin, A. L. *J. Mol. Struct. (THEOCHEM)* **1991**, *251*, 1.
(12) Schaeffer, T.; Penner, G. H. *J. Mol. Struct. (THEOCHEM)* **1987**, *152*, 179.
(13) Velino, B.; Melandri, S.; Caminati, W.; Favero, P. G. *Gaz. Chim. Ital.* **1995**, *125*, 373.
(14) Oikawa, A.; Abe, H.; Mikami, N.; Ito, M. *Chem. Phys. Lett.* **1985**, *116*, 50.
(15) Yamamoto, S.; Okuyama, K.; Mikami, N.; Ito. M. *Chem. Phys. Lett.* **1986**, *125*, 1.
(16) Breen, P. J.; Bernstein, E. R.; Secor, H. V., Seeman J. I. *J. Am. Chem. Soc.* **1989**, *111*, 1958.
(17) Cockett, M. C. R.; Takahashi, M.; Okuyama, K.; Kimura, K. *Chem. Phys. Lett.* **1991**, *187*, 250.
(18) Tsutsumi, K.; Sato, S.; Kimura, K. To be published.
(19) Cockett, M. C. R.; Okuyama, K.; Kimura, K. *J. Chem. Phys.* **1992**, *97*, 4679.
(20) Ito, M.; Takazawa K.; Fujii M. *J. Mol. Struct.* **1993**, *292*, 9.
(21) Takazawa K.; Fujii M.; Ebata, T.; Ito, M. *Chem. Phys. Lett.* **1992**, *189*, 592.
(22) Lu, K.-T.; Eiden, G. C.; Weisshaar, J. C. *J. Phys. Chem.* **1992**, *96*, 9742.
(23) Müller-Dethlefs, K.; Sander, M.; Schlag, E. W. *Z. Naturforsch. A* **1984**, *39*, 1089.
(24) Müller-Dethlefs, K.; Sander, M.; Schlag, E. W. *Chem. Phys. Lett.* **1984**, *112*, 291.
(25) Kimura, K.; Takahashi, M. *Optical Methods for Time- and State-Resolved Chemistry*; Ng, C. Y., Ed.; SPIE−The International Society for Optical Engineering: Bellingham, WA, 1992; Vol. 1638, p 216.

(26) Takahashi, M.; Ozeki, H.; Kimura, K. *Chem. Phys. Lett.* **1991**, *181*, 255.
(27) Takahashi, M.; Kimura, K. *J. Chem. Phys.* **1992**, *97*, 2920.
(28) Okuyama, K.; Cockett, M. C. R.; Kimura, K. *J. Chem. Phys.* **1992**, *97*, 1649.
(29) Takahashi, M.; Ozeki, H.; Kimura, K. *J. Chem. Phys.* **1992**, *96*, 6399.
(30) Cockett, M. C. R.; Kimura, K. *J. Chem. Phys.* **1994**, *100*, 3429.
(31) Dyke, J. M.; Ozeki, H.; Takahashi, M.; Cockett, M. C. R.; Kimura, K. *J. Chem. Phys.* **1992**, *97*, 8926.
(32) Araki, M.; Sato, S.; Kimura, K. *J. Phys. Chem.* **1996**, *100*, 10542.
(33) Vondrak, T.; Sato, S.; Kimura, K. *Chem. Phys. Lett.* **1996**, *261*, 481.
(34) Vondrak, T.; Sato, S.; Kimura, K. *J. Phys. Chem. A* **1997**, *101*, 2384.
(35) Wiley: W. C.; McLaren, I. H. *Rev. Sci. Instrum.* **1955**, *26*, 1150.
(36) Sato, S.; Kimura, K. *Chem. Phys Lett.* **1996**, *249*, 155.
(37) Frisch, M. J.; Trucks G. W.; Schlegel, H. B.; Gill, P. M. W.; Johnson, B. G.; Robb, M. A.; Cheeseman, J. R.; Keith, T. A.; Petersson, G. A.; Montgomery, J. A.; Raghavachari, K.; Al-Laham, M. A.; Zakrzewski, V. G.; Ortiz, J. V.; Foresman, J. B.; Cioslowski, J.; Stefanov, B. B.; Nanayakkara, A.; Challacombe, M.; Peng, C. Y.; Ayala, P. Y.; Chen, W.; Wong, M. W.; Andres, J. L.; Replogle, E. S.; Gomperts, R.; Martin, R. L.; Fox, D. J.; Binkley, J. S.; Defrees, D. J.; Baker, J.; Stewart, J. P.; Head-Gordon, M.; Gonzales, C.; Pople, J. A. *Gaussian 94* (Revision C. 3); Gaussian Inc.: Pittsburgh, PA, 1995.
(38) Cooley, J. W. *Math. Comput.* **1961**, *15*, 363.
(39) Spirko, V.; Kraemer, W. P.; Chejchan, A. *J. Mol. Spectrosc.* **1989**, *136*, 340.
(40) Ramaekers, J. J. F.; van Dijk, H. K.; Langelaar, J.; Rettschnick, R. P. H. *Faraday Discuss. Chem. Soc.* **1983**, *75*, 183.
(41) Brumbaugh, D. V.; Kenny, J. E.; Levy, D. H. *J. Chem. Phys.* **1983**, *78*, 3415.
(42) Menapace, J. A.; Bernstein, E. R. *J. Phys. Chem.* **1987**, *91*, 2533.
(43) Jacobson, B. A.; Humphrey, S.; Rice, S. A. *J. Chem. Phys.* **1988**, *89*, 5624.
(44) Weber, P. M.; Buontempo, J. T.; Novak, F.; Rice, S. A. *J. Chem. Phys.* **1988**, *88*, 6082.
(45) Weber, P. M.; Rice S. A. *J. Chem. Phys.* **1988**, *88*, 6107.
(46) Shinohara, H.; Sato, S.; Kimura, K. *J. Phys. Chem.*, in press.
(47) Yamanouchi, K.; Isogai, S.; Tsuchiya, S.; Kuchitsu, K. *Chem. Phys. Lett.* **1987**, *116*, 123.
(48) Amirav, A.; Even, U.; Jortner, J.; Dick, B. *Mol. Phys.* **1983**, *49*, 899.